remote sensing

MDPI

Article

Timely and Low-Cost Remote Sensing Practices for the Assessment of Landslide Activity in the Service of Hazard Management

Aggeliki Kyriou, Konstantinos G. Nikolakopoulos * and Ioannis K. Koukouvelas

Department of Geology, University of Patras, 265 04 Patras, Greece
* Correspondence: knikolakop@upatras.gr

Abstract: Landslides are among the most dangerous and catastrophic events in the world. The increasing progress in remote sensing technology made landslide observations timely, systematic and less costly. In this context, we collected multi-dated data obtained by Unmanned Aerial Vehicle (UAV) campaigns and Terrestrial Laser Scanning (TLS) surveys for the accurate and immediate monitoring of a landslide located in a steep and v-shaped valley, in order to provide operational information concerning the stability of the area to the local authorities. The derived data were processed appropriately, and UAV-based as well as TLS point clouds were generated. The monitoring and assessment of the evolution of the landslide were based on the identification of instability phenomena between the multi-dated UAV and TLS point clouds using the direct cloud-to-cloud comparison and the estimation of the deviation between surface sections. The overall evaluation of the results revealed that the landslide remains active for three years but is progressing particularly slowly. Moreover, point clouds arising from a UAV or a TLS sensor can be effectively utilized for landslide monitoring with comparable accuracies. Nevertheless, TLS point clouds proved to be denser and more appropriate in terms of enhancing the accuracy of the monitoring process. The outcomes were validated using measurements, acquired by the Global Navigation Satellite System (GNSS).

Keywords: landslide mapping; landslide monitoring; UAV; terrestrial laser scanning; 3D point clouds

Citation: Kyriou, A.; Nikolakopoulos, K.G.; Koukouvelas, I.K. Timely and Low-Cost Remote Sensing Practices for the Assessment of Landslide Activity in the Service of Hazard Management. *Remote Sens.* **2022**, *14*, 4745. https://doi.org/10.3390/rs14194745

Academic Editor: Christian Bignami

Received: 18 August 2022
Accepted: 19 September 2022
Published: 22 September 2022

1. Introduction

Landslides are among the most dangerous and catastrophic natural disasters in the world. They usually occur suddenly and can be detrimental to the natural environment, the infrastructure or even human life itself. As climate change is unequivocal, model-based estimations propose that warming temperatures would lead to increased activity of landslides [1–3]. Over the years, several researchers dealt with the investigation of such phenomena and various methods focused on landslide vulnerability mapping, hazard zoning, risk assessment, or rock-fall simulations, have been developed [4,5]. However, landslide research has never been more urgent and important.

The increasing progress in remote sensing technology have made landslide observations more timely, systematic and less costly. Moreover, new possibilities for high-precision research of landslides located in inaccessible areas or extensive landslides have emerged. Novel methodologies, based on multiple remote sensing data, have already been indispensable tools for landslide assessment and risk prevention [6,7].

The growing use of Unmanned Aerial Vehicles (UAVs) has been a real milestone in Earth observation, and therefore, in landslide research [8,9]. The first approaches were based on the successful exploitation of UAVs with compact cameras for the rapid identification of landslides [10]. Subsequently, UAVs mounted with digital single-lens reflex (DSLR) cameras, were used for the documentation and monitoring of large earthflows [11]. An academic research team developed a UAV, equipped with a consumer-grade optical camera in order to generate 3D surface models for the more comprehensive characterization and monitoring of unstable areas [12].

Moreover, time series of UAV images were processed via the Structure from Motion (SfM) technique and the outputs were utilized for the quantification of the surface deformation, the measurement of the landslide volumetric change and the determination of the landslide's dynamics [13,14]. In a respective study, UAV data contributed effectively to the assessment of residual risk (post-landslide risk) on a medium- and long-term scale through the estimation of the evolution of the area [15]. UAV imagery along with digital photogrammetry has successfully assisted in the recording of slope conditions as well as in the enhancement of the understanding of landslide processes and the precise assessment of slope instabilities [16]. As time passes, new and more innovative approaches for landslide investigation are emerging based on the combined use of UAVs and machine learning algorithms for the extraction of landslide susceptibility maps and the monitoring of landslide risk areas [17].

Another common tool for many geotechnical studies and landslide investigations is Light Detection and Ranging (LiDAR) technology [18]. In particular, Airborne LiDARs have proven to be particularly effective in the detailed and accurate representation of the landslide's surface, the recognition of different types of mass movements and the monitoring of landslide dynamics as well as the classification of slow-moving landslides in densely vegetated areas [19–22]. In addition, a variety of studies have already been carried out regarding the utilization of LiDARs on rockfall mapping, rock mass characterization and rockfall susceptibility analysis [23,24]. However, landslide research through airborne LiDAR constitutes a quite expensive approach and thus continuous airborne monitoring is relatively limited.

On the contrary, Terrestrial LiDAR (TLS) surveys are more affordable, providing data with a higher temporal and spatial resolution. An overall overview of TLS acquisition and data processing concerning the characterization, volume estimation and monitoring of rock slopes has already been published [25]. Furthermore, a truly comprehensive study took place in Yosemite Valley where TLS and SfM were utilized for the detection of rockfalls over a 40-year period and the updating of the inventory database with more precise measurements (number, area, volume) [26]. In fact, the terrain models resulting from remote sensing techniques (TLS, SfM) were compared with the corresponding models derived from the processing of historical oblique photographs allowing the detection and quantification of surface changes and providing long-term monitoring.

The integrated use of a variety of remote sensing data is suggested as an alternative perspective for more comprehensive landslide research. Specifically, spaceborne satellite data (high resolution multispectral and radar images) were combined with UAV imagery and ground-based techniques, such as Ground-Based Interferometric SAR (GB-InSAR), TLS, etc., in order to identify, map and monitor landslides, which vary in their characteristics, failure mechanisms, evolution processes, spatial distribution and risk of instability [27]. Moreover, the analysis of the activity of the landslide and the estimation of its kinematic evolution can be achieved effectively either by the execution of repeated UAV campaigns along with Global Navigation Satellite Systems (GNSS) surveys [28] or by the utilization of UAV data in conjunction with (a) airborne LiDAR data [29] or (b) TLS surveys [30].

In the current study, we collected multi-dated data obtained by Unmanned Aerial Vehicle (UAV) and Terrestrial Laser Scanning (TLS) surveys for the accurate and immediate monitoring of a landslide aiming at the provision of operational information concerning the stability of the area to the local authorities. Specifically, a landslide occurred in an environmentally sensitive area, which is located in a steep and narrow valley. Thus, the monitoring of the area constitutes a particularly challenging task, as it must be achieved timely and accurately with as little environmental impact as possible and minimum costs. As both UAV and TLS field campaigns involve only transportation expenses to the study area, they have proved to be a reliable and cost affordable tool for continuous monitoring of small (ten of meters) to moderate (hundreds of meters) active landslides. The aforementioned challenge is the main objective of the current work. In this framework, the derived data were processed appropriately, and UAV-based as well as TLS point clouds

were generated. The monitoring and assessment of the evolution of the landslide were based on the identification of instability phenomena between the multi-dated UAV and TLS point clouds using the direct cloud-to-cloud comparison and the estimation of the deviation between surface sections. Moreover, systematic measurements, obtained by the Global Navigation Satellite System (GNSS) were utilized for the verification of the results. Finally, research outcomes were communicated to local authorities in order to execute appropriate measures for the mitigation of the risk.

2. Landslide Area

Northern Peloponnese is characterized as one of the most tectonically and seismically active continental regions worldwide due to the existence of the fast-extending Corinthian rift [31–35]. The rift is dissecting the entire region, from the coastline in the north to the ridges inland since the Pliocene. Normal faulting, sea level changes, as well as the tectonic uplift of rift sediments, are recognized as dominant features in this process. The morphology of the wider area is obviously affected by the ongoing tectonics and it is evidenced by the development of deep and narrow valleys.

Our area of interest is located on the outskirts of the village of Kato Zachlorou within the Region of Western Greece (Figure 1). The first phenomena of instability at the specific site started as rock falls on 19 April 2019. A subsequent reactivation took place on 14 November 2019 through rockfalls and debris falls, while a more extensive event, including rock falls and debris falls occurred on 4 April 2020. Landslide material covered the area of the road in three different locations, contributing to the isolation of the local community from the surroundings (Figure 2).

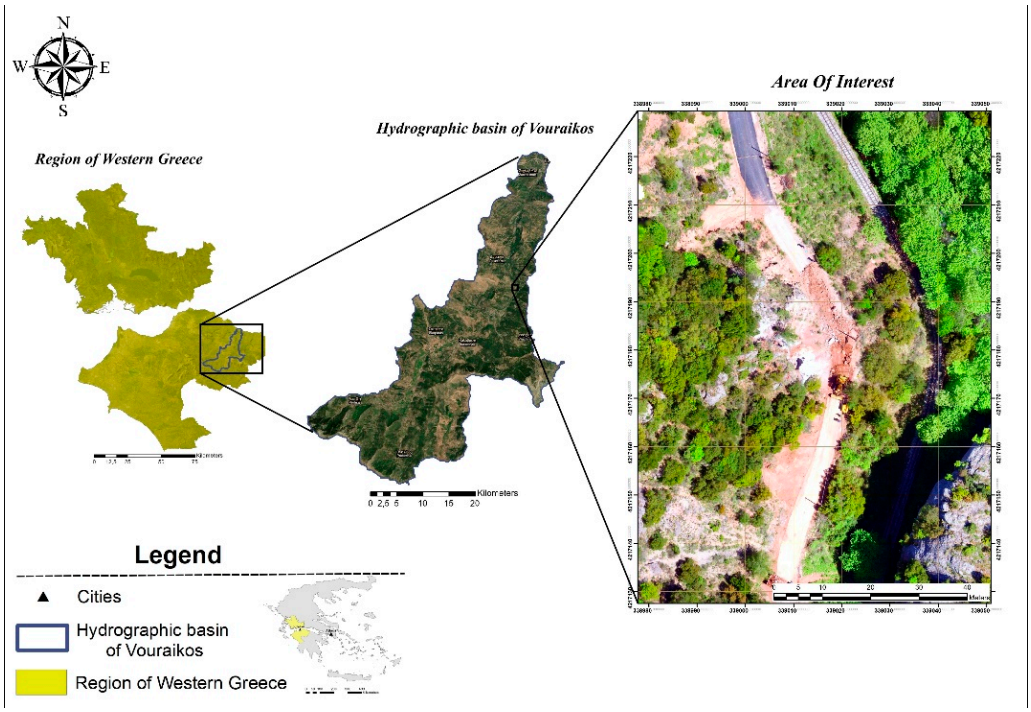

Figure 1. Area of Interest.

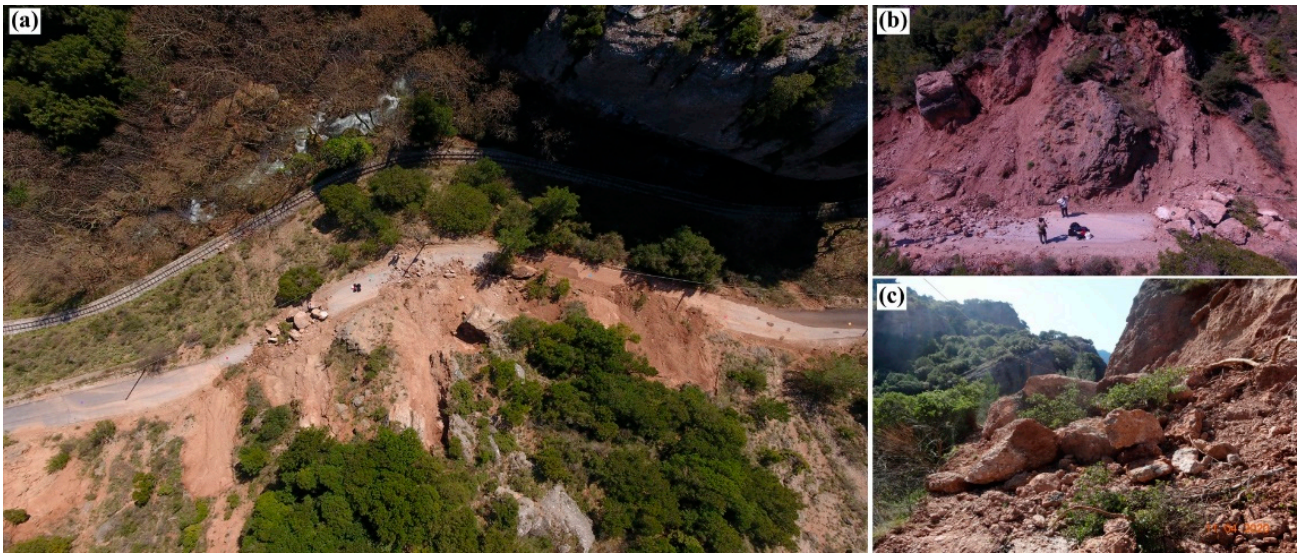

Figure 2. (**a**,**b**) UAV photos of the area of interest after the landslide on 4 April 2020. (**c**) Photo of the landslide material displaced on the area of the road.

The specific site is an outstanding natural heritage area, as well as a famous tourist destination. A historic rack railway, named "Odontotos" runs through the gorge of Vouraikos since 1896 and it is one of the most iconic touristic features of the wider area. In this context, the mitigation of landslide risk and the maintenance of human security are top priorities, especially in our area of interest, which is located in a particularly narrow area of the gorge and quite close to the railway lines (~30 m) (Figure 2a). Additionally, this environmentally sensitive area must be safeguarded and thus any monitoring should take place with as little environmental disturbance as possible.

3. Materials and Methods

3.1. Data Acquizition

The precise monitoring of our area of interest started after the occurrence of the extensive rock falls and debris fall on 19 April 2019 and is still in progress. Our datasets included repetitive representations of the study area acquired by either UAV or by TLS as well as high-precision GNSS measurements (Table 1). Repeated UAV/TLS surveys have been carried out at regular intervals for the immediate provision of stability information to the local authorities. UAV flights are operated within 1 h while each TLS survey lasts approximately 4 h.

A DJI Matrice 600 was utilized for the collection of the UAV imagery. The specific hexacopter is equipped with a Zenmuse X5 camera with a 15 mm F/1.7 lens and a 72-degree diagonal field of view. The camera operates with an electronic shutter, capturing images at 16 MP analysis, i.e., photo analysis of 4608 × 3456 pixels. The campaigns were executed once per month at an altitude of 70 m above the ground level, maintaining the same flight grid (Figure 3) and the corresponding photogrammetric characteristics throughout the monitoring period. The acquired UAV photos have 90% along-track and 75% across-track overlap and photogrammetric processing was carried out in Agisoft Metashape software.

TLS surveys were conducted using a Leica ScanStation P50, which allows the extremely fast scanning (1 million points per second) of large areas along with the extraction of high-quality 3D representations. The range accuracy of the specific laser scanner is estimated at about 1.2 mm for ranges varying from 120 m to 270 m. In addition, scanning can be performed under almost any weather conditions (exceptions include stormy winds and heavy rainfall) in a 360-degree horizontal and 270-degree vertical field of view. A Canon EOS 80D camera with 24 MP resolution is mounted onto Leica ScanStation P50

for the improvement of the sharpness of the obtained point clouds. The processing of the multi-dated point clouds took place in Leica Cyclone software.

Table 1. Dates of the repeated UAV, TLS and GNSS surveys.

Survey	Date	UAV	TLS	GNSS	Main Events
	19 April 2019				Rock falls
1	21 April 2019	X			
2	19 May 2019	X			
	14 November 2019				Rock falls and earth slides
	4 April 2020				Extensive rock falls and earth slides
3	11 April 2020	X			
4	7 May 2020	X			
5	10 June 2020	X	X		
	22 July 2020				Slope remediation
6	23 July 2020	X			
	24 July 2020				Construction of GNSS pillars
7	10 August 2020	X		X	
8	14 August 2020	X		X	
9	25 August 2020	X		X	
10	25 September 2020	X	X	X	
11	3 October 2020	X		X	
12	16 December 2020	X		X	
13	26 April 2021	X		X	
14	28 May 2021	X		X	
15	3 July 2021	X		X	
16	7 November 2021	X	X	X	

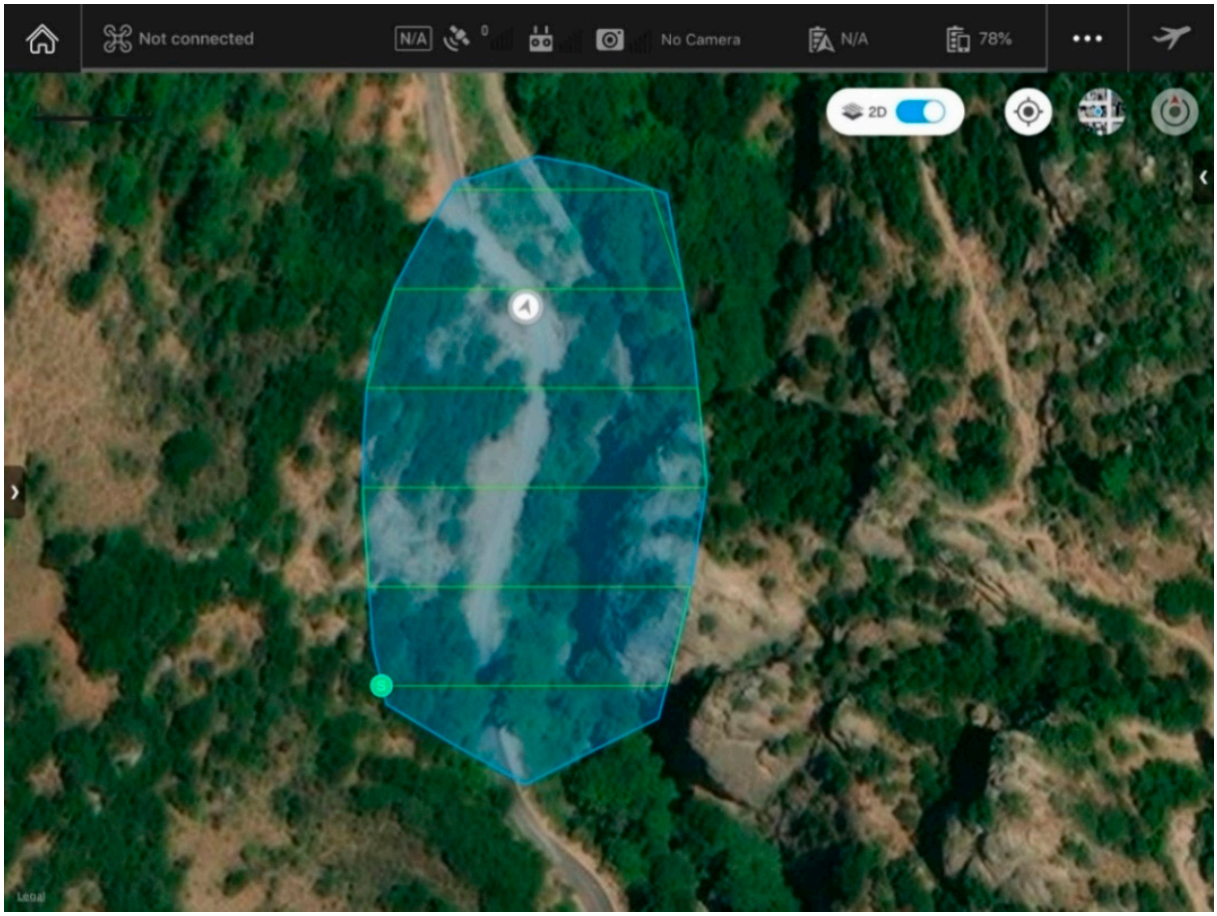

Figure 3. The flight grid of the photogrammetric UAV campaigns.

Moreover, several repetitive static GNSS measurements were executed utilizing a Leica GS08 GNSS Receiver. The adopted methodology for the construction of the permanent GNSS pillar and the and subsequent monitoring has already been described in detail [28]. The measurements were performed on permanent pillars (Figure 4), which are located at key points within the area of interest in order to guarantee the performance of each measurement exactly at the same position. In particular, three of these permanent pillars were constructed along the paved road, while two others were placed outside the landslide. GNSS measurements were utilized both to monitor instability phenomena and to verify the results of remote sensing approaches.

Figure 4. Permanent location on the road area for the execution of GNSS measurements.

Finally, square 4.5″ black and white targets were distributed throughout the area of instability (Figure 5) in each UAV campaign or TLS survey, aiming at minimizing georeferencing errors and enhancing the registration quality of the multi-dated outputs. The position of each target was measured using a Leica GS08 GNSS Receiver.

3.2. Methodology

The current research focuses on the accurate and timely monitoring of landslide activity using low-cost, repeatable remote sensing data obtained by UAV and TLS sensors, in an environmentally sensitive area. Our main purpose is to inform the local authorities about the stability of the area, within two days (maximum) from the field surveys, in order to respond immediately by planning the appropriate measures, in case of a possible emergency (future landslide). An overview of the adopted methodology is shown in the following flowchart (Figure 6). The validation of the results takes place through their comparative assessment with GNSS measurements, performed on permanent positions (Figure 7).

Figure 5. (**a**) Distribution of GCPs in the area of interest, (**b**) 4.5″ black and white target, (**c**) 4.5″ black and white target within the landslide area.

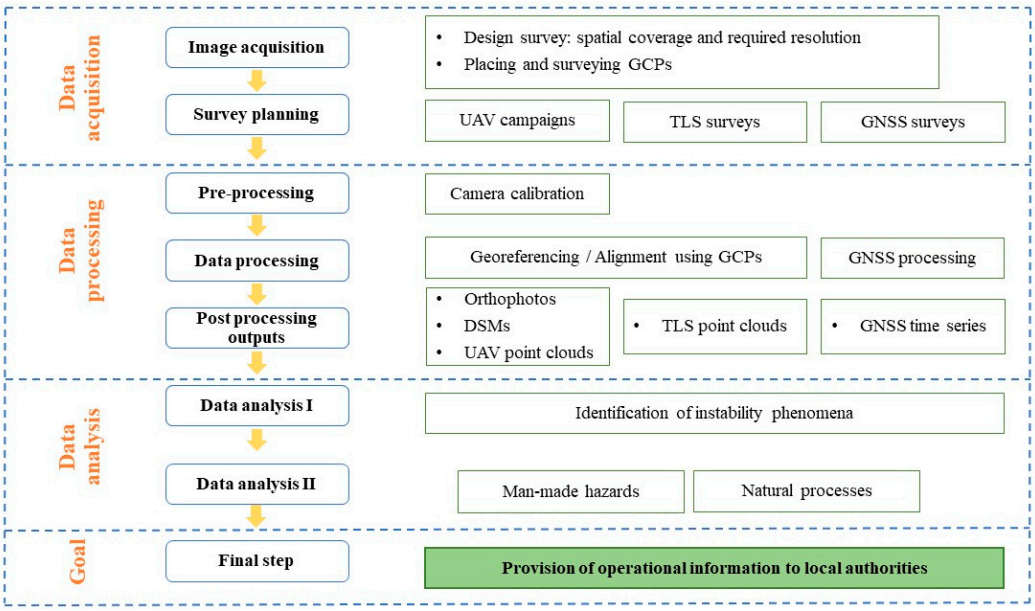

Figure 6. Flowchart depicting the applied methodology.

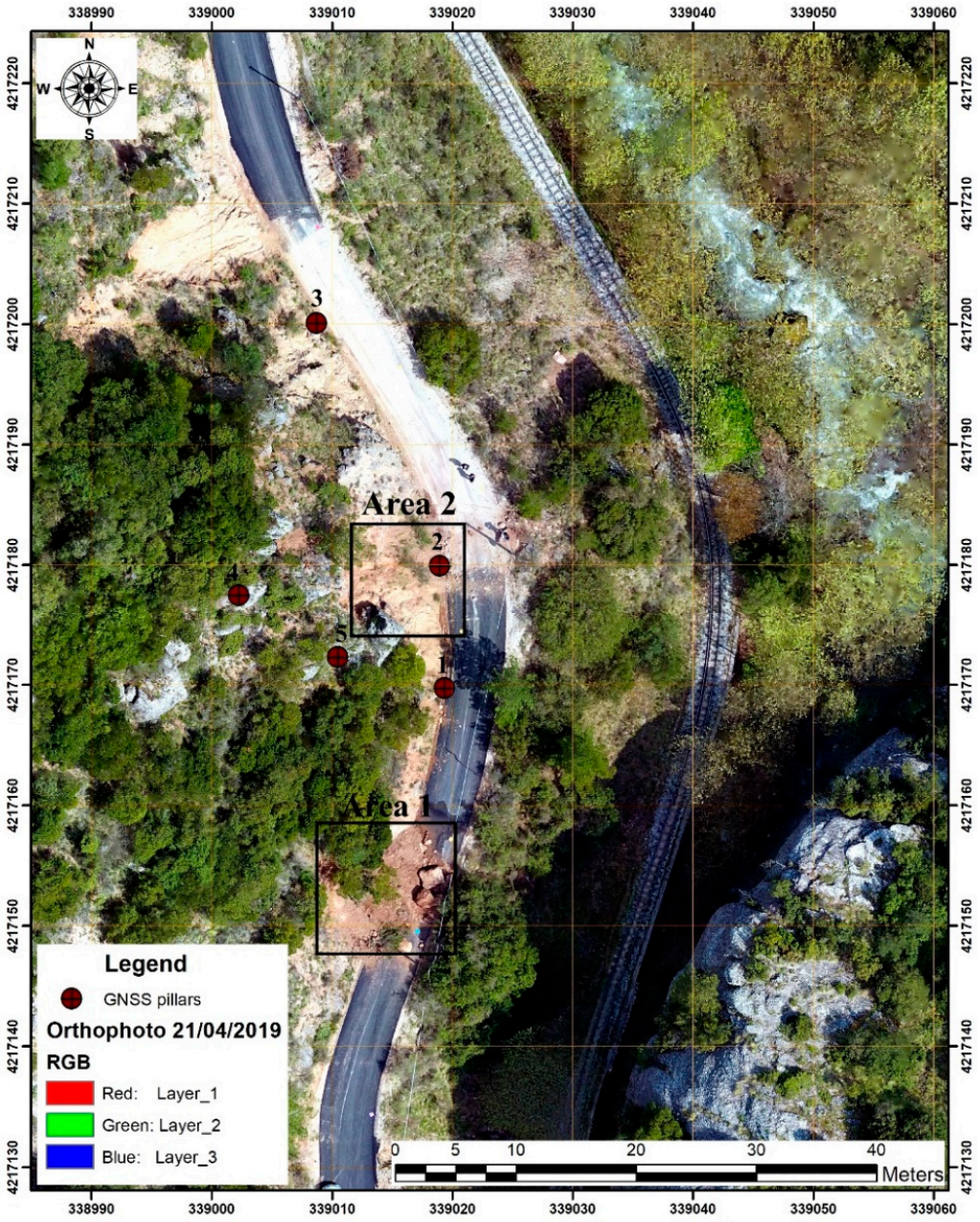

Figure 7. Distribution of the GNSS permanent pillars. The orthophoto presents the sliding area on 21 April 2019.

Specifically, the obtained UAV images were processed in Agisoft Metashape (v. 1.7.2., Agisoft LLC, St. Petersburg, Russia) according to the SfM photogrammetry. The technique transforms the overlapping, multi-view UAV images into a three-dimensional object model [36–38]. The origin of SfM is traced to the fields of computer vision and photogrammetry. In our case, the UAV images were aligned using the highest-quality option as described in the Agisoft Metashape manual [39]. The specific option is inextricably linked to the quality of the 3D reconstruction since the camera positions are calculated more accurately. In addition, the collected images were processed in their original size and at the same time, they were upscaled by a factor of 4. The dense point cloud generation was performed according to the ultra-high-quality setting which allows for the creation of more detailed and precise depth maps. Concerning the camera calibration and optimization, the default setting of Agisoft Metashape was selected. The SfM processing ended up in

the extraction of point clouds, which were projected into the Hellenic Geodetic Reference System 1987.

The processing of the indicative TLS data was carried out in Leica Cyclone software. Six scan stations were required in each TLS survey to fully cover the area of interest. Therefore, the primary step of the processing was the correct registration of the scans obtained by the different scan positions. The procedure took place using Leica Cyclone REGISTER 360 through the identification of the 4.5″ black and white targets. The registration error in the specific step was measured at 6 mm. Afterward, the multi-dated point clouds were imported into Leica Cyclone REGISTER in order to be properly aligned. The alignment was executed through the detection of common points between the point clouds. The derived TLS three-dimensional representations along with the corresponding UAV-based point clouds were utilized for the monitoring of the landslide's evolution

4. Results

4.1. UAV Surveys

The systematic monitoring of mass movements across the investigated area using UAV imagery was based on change detection approaches. Specifically, high-resolution orthophotos were utilized for the visual identification of surface changes between the repetitive sliding episodes. Some typical relief changes, detected between the first mass movements in April 2019 (Table 1) and the more extensive ones in April 2020, are presented in Figure 8. Specifically, Figure 8a,b show area 1 between the two episodes, while Figure 8c,d correspond to area 2. In both cases, the crosshair is located in the same position. As can be observed, instabilities were evolving as evidenced by the displacement of large conglomerate boulders and soil towards the area of the road as well as vegetation changes.

Figure 8. Orthophotos: (**a**) Area 1 on 11 April 2020, (**b**) Area 1 on 21 April 2019, (**c**) Area 2 on 11 April 2020, (**d**) Area 2 on 21 April 2019.

Local authorities after the occurrence of the extensive mass movements (April 2020) decided to execute some stabilization measures in order to reduce the risk. Operations took place in late July 2020 and included scaling and trimming of the overhanging conglomerates. Therefore, the evolution of the topography of the investigated area from April 2020 to the end of 2021 is strongly related to man-made activities as well as natural processes.

The derived products of UAV photo processing were used for monitoring the topographic variation arising from both factors. In fact, multi-dated orthophotos, covering the investigated area, were exploited for the determination of the areas of instabilities through the monitoring of the vegetation evolution (Figure 9). The initial extent of the mass movements is displayed in blue, whilst the corresponding boundary of November 2021 is shown in red. The lines present significant changes, which are expressed by local vegetation variations and they are related to stabilization operations. Relief modifications related to the specific operations are equally obvious in surface profiles derived from UAV's DSMs (Figure 10). The surface profile of April 2019 is shown in magenta, while the respective profile after the remediation of the slope is depicted in red.

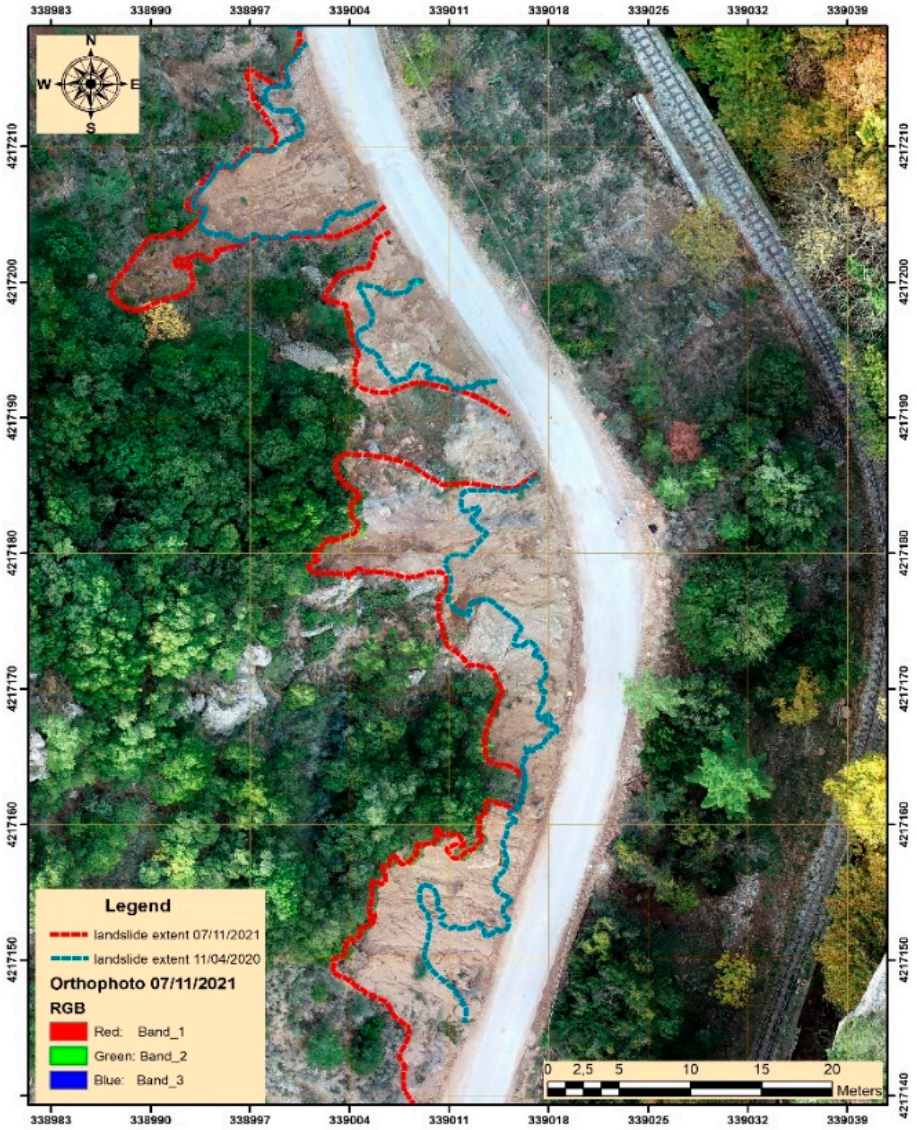

Figure 9. Evolution of the extent of the mass movements over time.

Concerning the monitoring of the instabilities using UAV point clouds, the processing relied on the direct cloud-to-cloud comparison, which was carried out in the Leica Cyclone 3DR extension. The results of this comparison, related to either manmade activities or natural processes are presented in Figure 11. In particular, UAV point clouds, obtained on 10 June 2020 and 25 September 2020 were exploited to detect relief variations that emerged from the stabilization measures (Figure 11a). The greatest changes were varying from 1.5 m to 1.7 m and were highlighted in reddish to magenta colors. Regarding the evolution of the mass movements influenced by natural processes, 3D point clouds acquired on 25 September 2020 and 7 November 2021 were compared (Figure 11b). Following this comparison, small, scattered surface variations were detected throughout the landslide. In the specific output, the topographic variations were overestimated concerning their distribution, which is associated with the sparser density of UAV point clouds and the temporal changes in vegetation. It is worth mentioning that in both periods, the surface changes depicted the dispersion area, despite the positive values that emerged from the processing procedure. Unfortunately, local authorities were removing the sliding materials daily in the area of the road, thus it is impossible to map the volume accumulated.

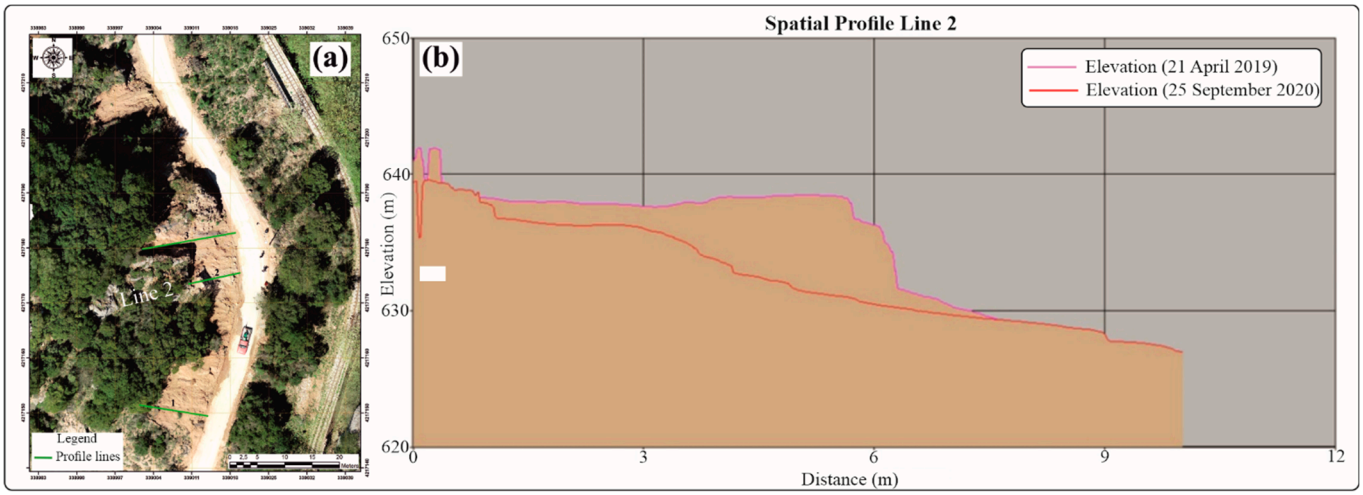

Figure 10. Surface profiles capturing relief modification after the stabilization operations. (**a**) Disribution of the profile sections within the area of interest. (**b**) Multitemporala surface profiles. The surface profile of April 2019 is shown in magenta, while the respective profile after the remediation of slope is depicted in red.

4.2. TLS Surveys

The detection of potential phenomena of instability within the area of interest, utilizing TLS surveys, was performed through cloud-to-cloud comparisons between the acquired multi-dated point clouds. In particular, TLS sensors are able to identify surface differences arising from manmade activities (Figure 12a) or natural processes (Figure 12b) in a more accurate way. The largest surface change associated with the stabilization measures was calculated at about 1.60 m and is close enough to the actual topographic modifications (Figure 12a). On the other hand, scattered relief changes related to erosion processes were noticed between the point clouds obtained on 25 September 2020 and 7 November 2021; they were estimated at about 0.5 m (Figure 12b). The procedure concerned the dispersion areas and not the areas of accumulation, as has already been noted.

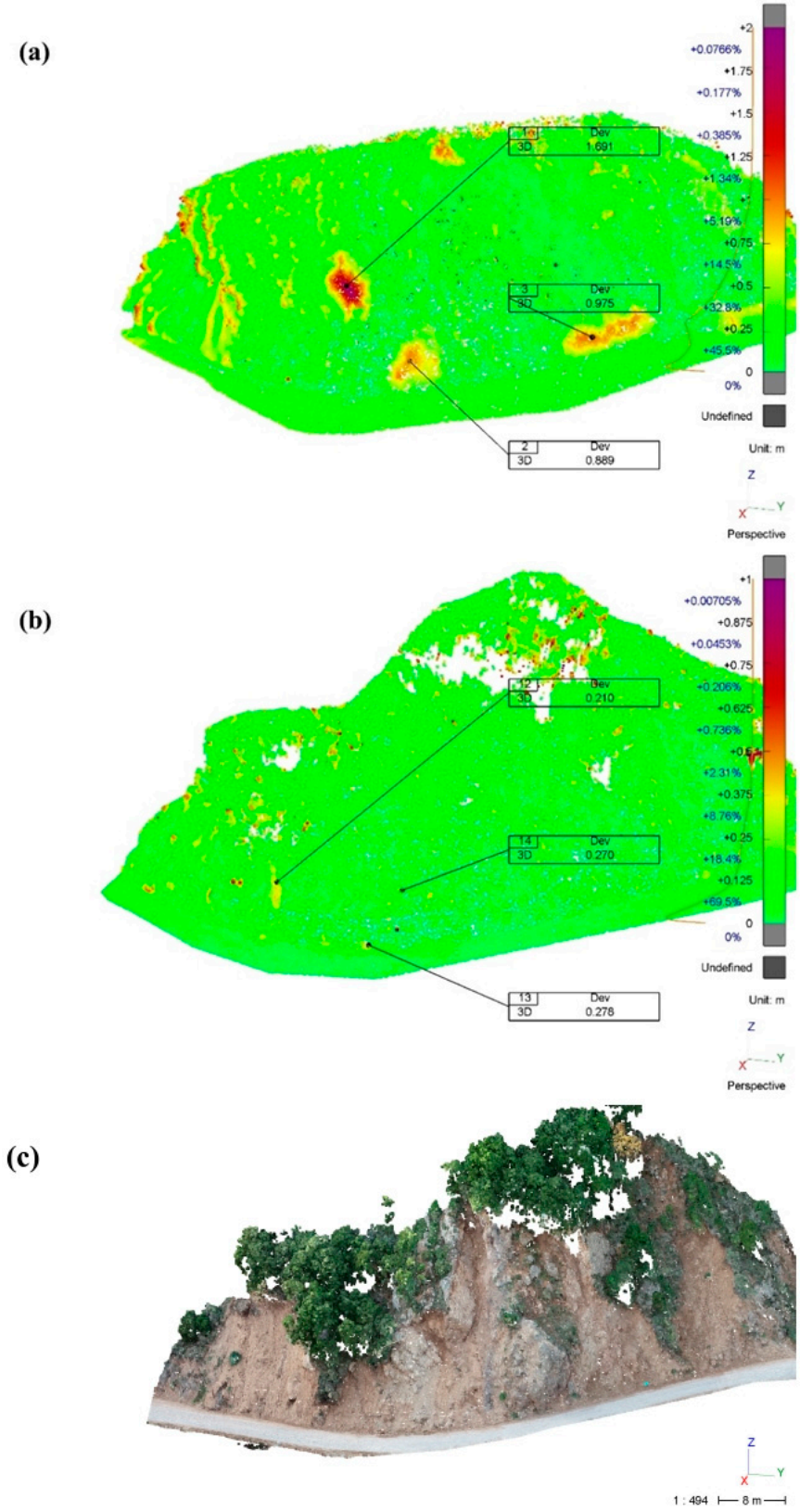

Figure 11. (**a**) Cloud-to-cloud comparison between the UAV point clouds, acquired on 10 June 2020 and 25 September 2020. (**b**) Cloud-to-cloud comparison between the UAV point clouds, acquired on 25 September 2020 and 7 November 2021. (**c**) UAV point cloud acquired on 25 September 2020 in RGB.

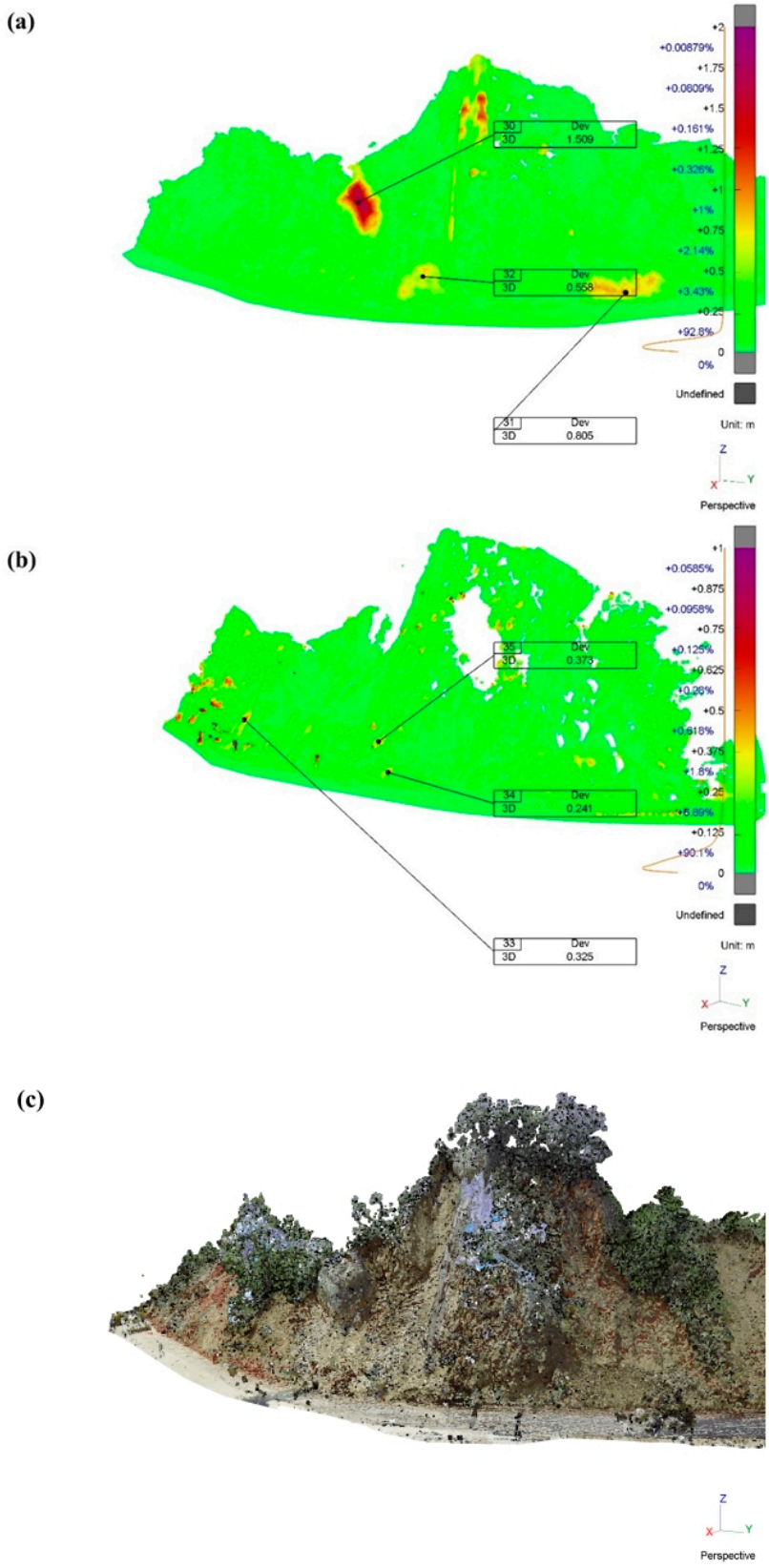

Figure 12. (**a**) Cloud-to-cloud comparison between the TLS point clouds acquired on 10 June 2020 and 25 September 2020. (**b**) Cloud-to-cloud comparison between the TLS point clouds, acquired on 25 September 2020 and 7 November 2021. (**c**) TLS point cloud acquired on 10 June 2020 in RGB.

Moreover, surface profiles of the multi-dated TLS 3D topographic representations were generated in the context of more comprehensive monitoring of the mass movements within the area of interest. Specifically, the intersection between the surface profiles of the TLS point clouds managed to capture accurately and efficiently the parts where the works for the remediation of the slope took place (Figure 13a). Red shades highlighted the areas where the greatest topographic changes have taken place due to the aforementioned operations. Although the output was expected, considering the accuracy of TLS data, it was truly surprising to discover that TLS sensors are able to detect micro-displacements associated with the particularly slow evolution of the topography of the area of interest (Figure 13b). The blue-green colors of the intersection depict the micro-displacements, while the road area seems to be lifting. In fact, these local surface changes, which emerged from the intersection of TLS surface profiles, were estimated at about 0.321 m and they have been confirmed by field observations and GNSS measurements (Table 2). These micro-displacements that indicate the ongoing activity of the slide, are easily observable in the contours of the multi-dated TLS representations, especially in the area of the road (Figure 14).

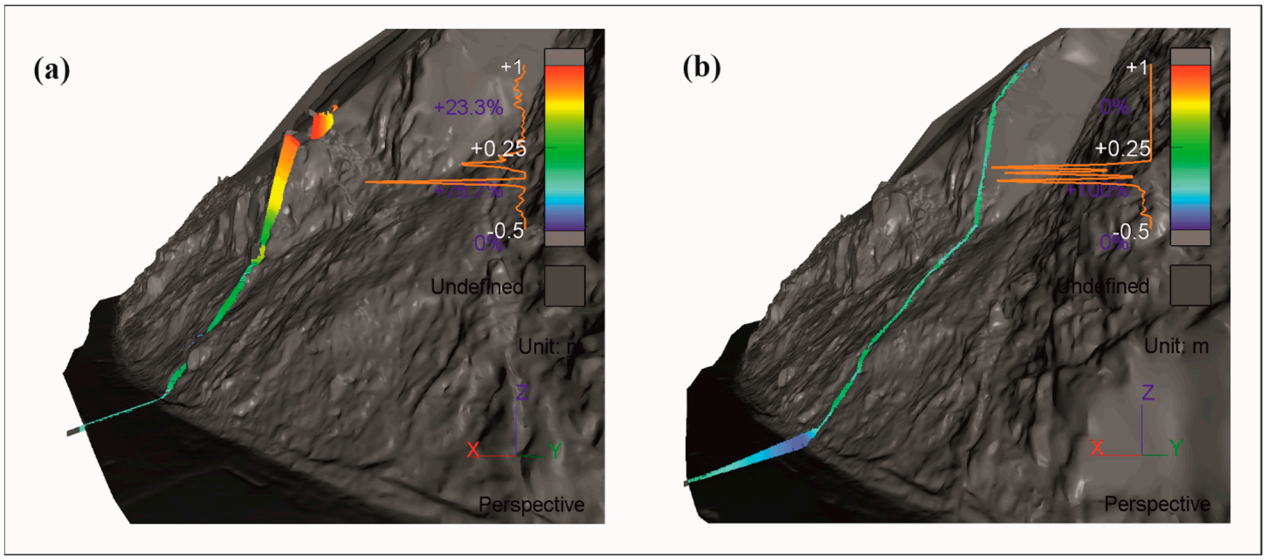

Figure 13. (**a**) Deviation between the surface sections of TLS point clouds acquired on 10 June 2020 and 25 September 2020. (**b**) Deviation between the surface sections of TLS point clouds, acquired on 25 September 2020 and 7 November 2021.

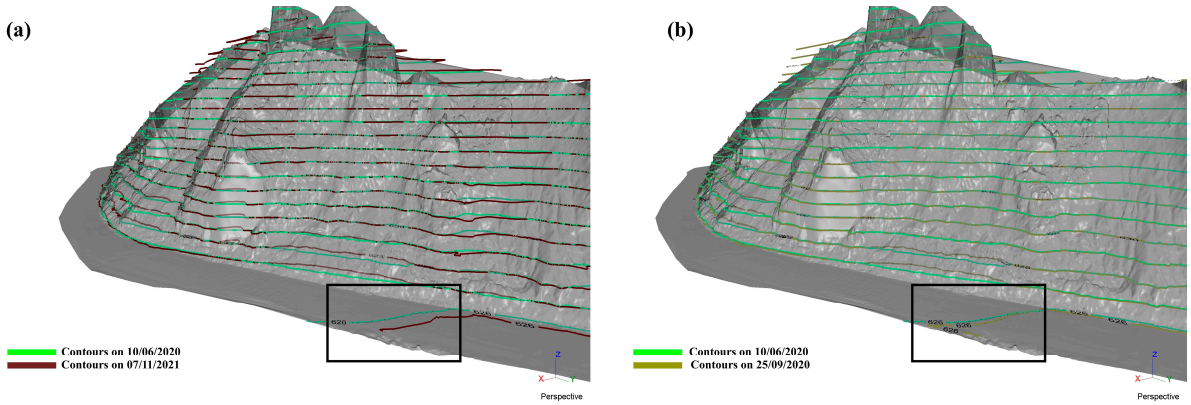

Figure 14. (**a**) Contours of the 3D TLS representations acquired on 10 June 2020 and 7 November 2021. (**b**) Contours of the 3D TLS representations acquired on 10 June 2020 and 25 September 2020. The black boxes surround the micro-movements along the road area.

Table 2. Surface deformation on permanent GNSS pillar 2.

Data Type	Surface Deformation (m)
GNSS measurements	0.334
UAV-based point clouds	0.203
TLS-based point clouds	0.312

4.3. Monitoring Overview and Computational Effort

As already mentioned, the main objective of this work is to provide information regarding the stability of the investigated area to the local authorities immediately, using low-cost and environmentally friendly approaches. The results demonstrated that UAVs, as well as TLS point clouds, are able to monitor the stability of the selected area precisely and effectively at regular intervals; local authorities have access to operational information about the selected site within 2 days.

In more detail, each UAV flight is performed in about 60 min and each scanning requires approximately 4 h for an 11,423 m^2 area with 120 m length (Table 3). The processing of the collected UAV and TLS data was performed in Agisoft Metashape and Cyclone software, respectively. The processing time for each approach is displayed in Table 3, while Table 4 contains the characteristics of the used computer. It is worth noting that TLS cloud density was particularly high between the repeated surveys, in contrast to the density of the UAV point clouds, which was obviously sparser. On the other hand, the increased and constant point density of the TLS point clouds is responsible for the good performance of the specific sensor even in the identification of micro-displacements. Furthermore, the operational cost of the applied approach is directly related only to the purchase of equipment and software or to repairing/upgrading issues.

Table 3. Characteristics and computational effort of UAV/TLS point clouds.

Sensor	Date	Point Cloud Density	Survey Time	Processing Time
UAV	10 June 2020	708.567 points	~60 min	~24 h
	25 September 2020		~60 min	~24 h
	7 November 2021		~60 min	~24 h
TLS	10 June 2020	6.000.000 points	~4 h	~12 h
	25 September 2020		~4 h	~12 h
	7 November 2021		~4 h	~12 h

Table 4. Characteristics of the used computer.

Processor	RAM	Disk	GPU
Intel Core i9 3.6 GHz	128 GB	SSD 1TB/HDD 2TB	NVIDIA GeForce RTX 3080

Meanwhile, we calculated the volume of these hanging rocks utilizing the point clouds obtained by either UAV or TLS, in the context of a comparison of the data used (Table 5). The calculation was carried out using the stockpile tools in Cyclone 3DR. Both approaches yielded similar results, which are slightly different from the assessment of the volume of the detached hanging rocks, as calculated by the local authorities. In particular, local authorities appointed staff from the Department of Geology of University of Patras, as consultants to monitor the instabilities within the area of interest [40]. In this framework, multi-dated UAV orthophotos and DSMs were imported into a GIS environment in order to calculate the volume of the hanging rocks. The estimation was based on simple mathematical operations between the digitized extents of the hanging rocks and the elevation differences. As can be observed, the specific estimation led to an overestimation of the volume, which is expected since the calculation took place in a rougher way. On the contrary, the proposed methodology, consisting of UAV and TLS surveys achieved a more realistic calculation of the volume with millimetric-scale accuracies.

Table 5. Estimation of the volume of the hanging rocks using UAV/TLS point clouds.

Data Type	Volume of the Hanging Rocks (m^3)
GIS methods	24.00
UAV-based point clouds	17.12
TLS-based point clouds	18.42

5. Discussion

Over the years, numerous researchers dealt with the investigation of landslides through the development of effective methodologies and tools for different aspects of landslide research, such as vulnerability mapping, risk assessment, etc. Nevertheless, proper landslide research has never been more urgent. New possibilities for landslide assessment and risk mitigation arose from the evolving development of technology and remote sensing. The aim of the current study is to provide the local authorities with useful and immediate operational information regarding the stability of an environmentally sensitive area while keeping at the same time operational costs as low as possible. On this basis, we performed multiple UAV flights and TLS surveys between April 2020 and November 2021. The collected UAV data were processed via SfM photogrammetry, resulting in the generation of multi-temporal point clouds. The accuracy assessment of the derived SfM products has already been examined in several studies using quantitative and qualitative methods along with a variety of reference data sets consisting of GNSS measurements, classical topographic measurements, etc. [41–43]. Most studies are emphasizing the effect of the number of GCPs and their distribution on the accuracy of the derived products [44–46]. Additionally, the registration and alignment of the TLS data led to the extraction of dense three-dimensional representations.

The monitoring and assessment of the landslide activity were carried out through the exploitation of the derived UAV-based point clouds and the respective TLS three-dimensional representations. TLS sensors have proven their effectiveness in the analysis of the spatio-temporal evolution of landslides in previous studies [47–49]. In this context, we tried to identify any surface change related to instability phenomena between the multi-dated UAV/TLS point clouds through the direct cloud-to-cloud comparison and the estimation of the deviation between surface sections. Surface variations emerging from either human activities or natural processes were successfully traced by both types of remote sensing data. The greatest surface modifications within the area of interest varied between 1.5 and 1.7 m; they were closely associated with the execution of the stabilization operations. Small, scattered surface displacements were detected throughout the area of interest during the last year as a result of erosion processes. Local authorities are constantly removing the newly induced sliding materials from the road area in order to keep the traffic flowing; however, this affects research in a way, as it only allows the mapping of the dispersion areas. In general, the outputs of the photogrammetric and the TLS processing were comparable; nevertheless, the evolution of the landslide area can be achieved more precisely (millimeter-scale) with the TLS-based point, as the corresponding UAV models were less accurate (centimeter-scale) due to the lower density of the point clouds (Table 3). Indeed, the micro-displacements which were observed in the TLS outputs (Figures 12–14), have been confirmed by field observations and the analysis of the GNSS measurements. In particular, Figure 15 depicted the x-, y-, z- coordinate variations of the permanent pillar 2 after the works for the remediation of the slope until now. The greatest differences vary between 0.1 m and 0.28 m. Therefore, it was demonstrated that the phenomena of instability within the area of interest were still ongoing until the end of 2021, but they are evolving slowly. We also have to mention that with the exception of the artificial boulder removal, all the other mass wasting over the slope is regularly distributed over the sliding area. These observations help the landslide classification as debris falls including minor conglomerate boulders. Similar methodologies based on cloud-to-cloud comparison have

been applied towards the determination of the deformation of active landslides or in other emergencies [50–52].

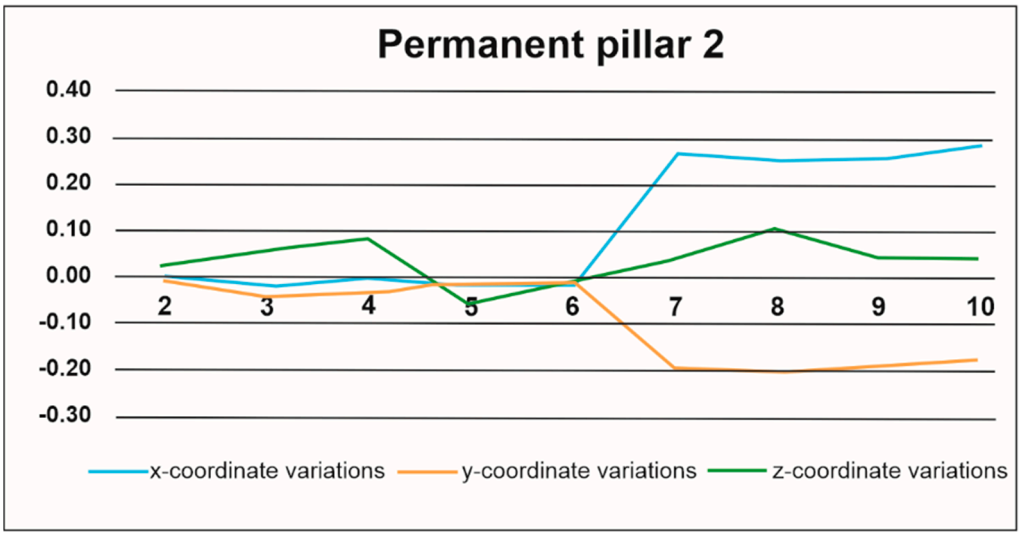

Figure 15. Variation of the coordinates of permanent pillar 2 over time. The *x*-axis corresponds to the period of GNSS measurements, while *y*-axis displays the observed displacements.

Many previous studies have examined the synergy of new technologies for landslide monitoring in conjunction with the minimization of operational costs. Synergistic use of TLS point clouds and GNSS measurements was proposed by [53] in order to map a landslide deformation in Puerto Rico. In order to reduce the high cost of purchasing commercial software, the specific study adopted the use of an open-source software package named Generic Mapping Tools for the processing of TLS data. Another study [54] proposes a combination of 12 low-cost single-frequency GNSS sensors, one seismometric station enhanced with another single-frequency GGNSS sensor and only one dual-frequency GNSS receiver established outside of the unstable area. The specific system provided daily information to the local stakeholders about the landslide movement. Another low-cost GNSS network was established by [55] composed of six sensors inside the landslide area and one outside to be used as a reference. Special attention was given to the logistic limitations (no electrical power, no Wi-Fi, etc.). The GNNS network results were analyzed with other data derived from boreholes, piezometers, inclinometers, crackmeters and meteorological stations. The supplementarity of TLS and UAV point clouds and the operational cost decrease with repeated UAV campaigns in areas with steep reliefs were also discussed [56]. Ref. [56] have emphasized the fact that in areas of very steep topography, the TLS data acquisition implies discontinuities in the point cloud and as a result, there is no homogeneous rendering over the broader area. This gap in point cloud data is filled with low-cost UAV campaigns. Similarly, it was mentioned that UAV campaigns at low altitudes and SfM photogrammetry can prevail over the visibility limitations that are present in land-based methodologies, such as TLS [57–59]. The TLS and UAV data combination for landslide monitoring in Brazil is presented in [60]. It is mentioned that the combination of those two methods presents great advantages over conventional, costly and time-consuming methods.

The current work proposes an effective methodology for the monitoring of challenging areas using low-cost data, acquired by UAVs and TLSs along with repetitive GNSS measurements. The total survey time (for both UAV and TLS) is only 5 h, while the processing of the collected data is carried out within 24 h. Thus, local authorities are informed about the stability of the landslide area, almost simultaneously with the monitoring procedure (within 2 days). The suggested methodology can be used as a guide for monitoring challenging sites or for the quick detection of surface/terrain changes in other emergencies. In more detail the main recommendations of the proposed methodology are:

- Monitoring of instabilities in environmentally sensitive areas can be implemented through repeated UAV and TLS surveys.
- Repeatability is determined by the activity of the instabilities.
- The installation of a permanent GNSS network is recommended. In particular, five permanent GNSS positions, installed in critical places, are sufficient for an area of approximately 1700 m^2. Generally, the number of permanent positions should be adjusted to the characteristics of the area under investigation.
- UAV surveys are able to detect topographic variation on the order of centimeters. On the other hand, TLS surveys can identify micro-displacements (millimetric-scale).
- The synergistic use of UAV and TLS data contributes to the enhancement of the spatial coverage and point density of UAV-based point clouds. This could be considered an ideal monitoring method for areas with complex topography.
- The presence of dense vegetation is an important challenge in the monitoring procedure. In the current research, we tried to reduce the influence of vegetation through the manual segmentation of UAV/TLS point clouds to contain as much topographical information as possible. Further research on the specific issue is needed.

6. Conclusions

The provision of operational information concerning the stability of an environmentally sensitive area to local authorities for the mitigation of the risk was the main objective of the current research. Based on this, the monitoring of the selected site was implemented using timely and low-cost remote sensing data. The appropriately processed multi-dated UAV-based point clouds and the respective TLS point clouds were submitted to comparison procedures aiming at the determination of the evolution of the landslide over time. Direct cloud-to-cloud comparison and the intersection between surface sections were exploited as change detection approaches. The overall evolution of the landslide is distinguished into two sub-periods: the one that was in line with human activities and the other emerging from natural processes, which are still in progress. Both types of data managed to trace the surface changes into the different sub-periods, proving that UAV and TLS data can be used effectively in emergencies and for the accurate landslide classification as debris falls. In fact, the outputs of the photogrammetric and the TLS processing were comparable. Specifically, the largest surface changes detected in UAV/TLS point clouds for the first monitoring period were varying between 1.5 m to 1.7 m. Additionally, the small local surface changes (0.20 m–0.30 m) which are identified on the sliding area during the second monitoring period—related to the natural processes—indicated that the landslide was still active until 11/2021, but it is evolving slowly. It is worth mentioning that the immediate and precise monitoring of the evolution of the landslide seems to be more efficient with the usage of the TLS-based point clouds, which are denser through the monitoring procedure. However, integrated use of UAV and TLS data could be suggested as a hybrid approach for the improvement of the spatial coverage and the point density of UAV-based point clouds. Eventually, this low-cost methodology can be utilized as a guide for the monitoring of challenging or sensitive sites or for the rapid detection of deformations arising from natural disasters or human activities.

Author Contributions: Conceptualization, K.G.N., I.K.K. and A.K.; methodology, K.G.N. and A.K.; software, K.G.N. and A.K.; validation, K.G.N., I.K.K. and A.K.; formal analysis, K.G.N., I.K.K. and A.K.; investigation, K.G.N., I.K.K. and A.K.; resources, K.G.N. and I.K.K.; data curation, K.G.N., I.K.K. and A.K.; writing—original draft preparation, K.G.N. and A.K.; writing—review and editing, K.G.N., I.K.K. and A.K.; visualization, K.G.N., I.K.K. and A.K.; supervision, K.G.N. and I.K.K.; project administration, K.G.N. and I.K.K.; funding acquisition, K.G.N. and I.K.K. All authors have read and agreed to the published version of the manuscript.

Funding: This research received no external funding.

Data Availability Statement: Data available on request due to restrictions. The data presented in this study are available on request from the corresponding author. The data are not publicly available due to public safety reasons.

Acknowledgments: The authors would like to thank Eidikos Logariasmos Kondilion kai Ereunas University of Patras for the support and the payment of the publication fees.

Conflicts of Interest: The authors declare no conflict of interest.

References

1. Gariano, S.L.; Guzzetti, F. Landslides in a changing climate. *Earth-Sci. Rev.* **2016**, *162*, 227–252. [CrossRef]
2. Huggel, C.; Khabarov, N.; Korup, O.; Obersteiner, M. Physical impacts of climate change on landslide occurrence and related adaptation. In *Landslides: Types, Mechanisms and Modeling*; Clague, J.J., Stead, D., Eds.; Cambridge University Press: Cambridge, UKI, 2012; pp. 121–133. [CrossRef]
3. Picarelli, L.; Lacasse, S.; Ho, K.K.S. The Impact of Climate Change on Landslide Hazard and Risk. In *Understanding and Reducing Landslide Disaster Risk*; Sassa, K., Mikoš, M., Sassa, S., Bobrowsky, P.T., Takara, K., Dang, K., Eds.; WLF 2020. ICL Contribution to Landslide Disaster Risk Reduction; Springer: Cham, Switzerland, 2021. [CrossRef]
4. Guzzetti, F.; Carrara, A.; Cardinali, M.; Reichenbach, P. Landslide hazard evaluation: A review of current techniques and their application in a multi-scale study, Central Italy. *Geomorphology* **1999**, *31*, 181–216. [CrossRef]
5. Mantovani, F.; Soeters, R.; Van Westen, C.J. Remote sensing techniques for landslide studies and hazard zonation in Europe. *Geomorphology* **1996**, *15*, 213–225. [CrossRef]
6. Lissak, C.; Bartsch, A.; De Michele, M.; Gomez, C.; Maquaire, O.; Raucoules, D.; Roulland, T. Remote Sensing for Assessing Landslides and Associated Hazards. *Surv. Geophys.* **2020**, *41*, 1391–1435. [CrossRef]
7. Zhong, C.; Liu, Y.; Gao, P.; Chen, W.; Li, H.; Hou, Y.; Nuremanguli, T.; Ma, H. Landslide mapping with remote sensing: Challenges and opportunities. *Int. J. Remote Sens.* **2020**, *41*, 1555–1581. [CrossRef]
8. Garnica-Peña, R.J.; Alcántara-Ayala, I. The use of UAVs for landslide disaster risk research and disaster risk management: A literature review. *J. Mt. Sci.* **2021**, *18*, 482–498. [CrossRef]
9. Gomez, C.; Purdie, H. UAV- based Photogrammetry and Geocomputing for Hazards and Disaster Risk Monitoring—A Review. *Geoenviron Disasters* **2016**, *3*, 23. [CrossRef]
10. Niethammer, U.; James, M.; Rothmund, S.; Travelletti, J.; Joswig, M. UAV-based remote sensing of the Super-Sauze landslide: Evaluation and results. *Eng. Geol.* **2012**, *128*, 2–11. [CrossRef]
11. Lindner, G.; Schraml, K.; Mansberger, R.; Hübl, J. UAV monitoring and documentation of a large landslide. *Appl. Geomat.* **2016**, *8*, 1–11. [CrossRef]
12. Rossi, G.; Tanteri, L.; Tofani, V.; Vannocci, P.; Moretti, S.; Casagli, N. Multitemporal UAV surveys for landslide mapping and characterization. *Landslides* **2018**, *15*, 1045–1052. [CrossRef]
13. Peppa, M.V.; Mills, J.P.; Moore, P.; Miller, P.E.; Chambers, J.E. Brief communication: Landslide motion from cross correlation of UAV-derived morphological attributes. *Nat. Hazards Earth Syst. Sci.* **2017**, *17*, 2143–2150. [CrossRef]
14. Turner, D.; Lucieer, A.; De Jong, S.M. Time Series Analysis of Landslide Dynamics Using an Unmanned Aerial Vehicle (UAV). *Remote Sens.* **2015**, *7*, 1736–1757. [CrossRef]
15. Godone, D.; Allasia, P.; Borrelli, L.; Gullà, G. UAV and Structure from Motion Approach to Monitor the Maierato Landslide Evolution. *Remote Sens.* **2020**, *12*, 1039. [CrossRef]
16. Rodriguez, J.; Macciotta, R.; Hendry, M.T.; Roustaei, M.; Gräpel, C.; Skirrow, R. UAVs for monitoring, investigation, and mitigation design of a rock slope with multiple failure mechanisms—A case study. *Landslides* **2020**, *17*, 2027–2040. [CrossRef]
17. Bernardo, E.; Palamara, R.; Boima, R. UAV and Soft Computing Methodology for Monitoring Landslide Areas (Susceptibility to Landslides and Early Warning). *Wseas Trans. Environ. Dev.* **2021**, *17*, 490–501. [CrossRef]
18. Jaboyedoff, M.; Oppikofer, T.; Abellán, A.; Derron, M.H.; Loye, A.; Metzger, R.; Pedrazzini, A. Use of LIDAR in landslide investigations: A review. *Nat. Hazards* **2012**, *61*, 5–28. [CrossRef]
19. Guo, C.; Xu, Q.; Dong, X.; Li, W.; Zhao, K.; Lu, H.; Ju, Y. Geohazard Recognition and Inventory Mapping Using Airborne LiDAR Data in Complex Mountainous Areas. *J. Earth Sci.* **2021**, *32*, 1079–1091. [CrossRef]
20. Mackey, B.H.; Roering, J.J.; McKean, J.A. Long-term kinematics and sediment flux of an active earthflow, Eel River, California. *Geology* **2009**, *37*, 803–806. [CrossRef]
21. Van Den Eeckhaut, M.; Kerle, N.; Poesen, J.; Hervás, J. Object-oriented identification of forested landslides with derivatives of single pulse LiDAR data. *Geomorphology* **2012**, *173–174*, 30–42. [CrossRef]
22. Ventura, G.; Vilardo, G.; Terranova, C.; Sessa, E.B. Tracking and evolution of complex active landslides by multi-temporal airborne LiDAR data: The Montaguto landslide (Southern Italy). *Remote Sens. Environ.* **2011**, *115*, 3237–3248. [CrossRef]
23. Fanos, A.M.; Pradhan, B. Laser Scanning Systems and Techniques in Rockfall Source Identification and Risk Assessment: A Critical Review. *Earth Syst Environ.* **2018**, *2*, 163–182. [CrossRef]
24. Guinau, M.; Tapia, M.; Pérez-Guillén, C.; Suriñach, E.; Roig, P.; Khazaradze, G.; Torné, M.; Royán, M.J.; Echeverria, A. Remote sensing and seismic data integration for the characterization of a rock slide and an artificially triggered rock fall. *Eng. Geol.* **2019**, *257*, 105113. [CrossRef]

25. Abellán, A.; Oppikofer, T.; Jaboyedoff, M.; Rosser, N.J.; Lim, M.; Lato, M.J. Terrestrial laser scanning of rock slope instabilities. *Earth Surf. Process. Landf.* **2014**, *39*, 80–97. [CrossRef]
26. Guerin, A.; Stock, G.; Radue, M.; Jaboyedoff, M.; Collins, B.; Matasci, B.; Avdievitch, N.; Derron, M.H. Quantifying 40 years of rockfall activity in Yosemite Valley with historical Structure-from-Motion photogrammetry and terrestrial laser scanning. *Geomorphology* **2020**, *356*, 107069. [CrossRef]
27. Casagli, N.; Frodella, W.; Morelli, S.; Tofani, V.; Ciampalini, A.; Intrieri, E.; Raspini, F.; Rossi, G.; Tanteri, L.; Lu, P. Spaceborne, UAV and ground-based remote sensing techniques for landslide mapping, monitoring and early warning. *Geoenviron. Disasters* **2017**, *4*, 9. [CrossRef]
28. Kyriou, A.; Nikolakopoulos, K.; Koukouvelas, I.; Lampropoulou, P. Repeated UAV Campaigns, GNSS Measurements, GIS, and Petrographic Analyses for Landslide Mapping and Monitoring. *Minerals* **2021**, *11*, 300. [CrossRef]
29. Pellicani, R.; Argentiero, I.; Manzari, P.; Spilotro, G.; Marzo, C.; Ermini, R.; Apollonio, C. UAV and Airborne LiDAR Data for Interpreting Kinematic Evolution of Landslide Movements: The Case Study of the Montescaglioso Landslide (Southern Italy). *Geosciences* **2019**, *9*, 248. [CrossRef]
30. Brook, M.S.; Merkle, J. Monitoring active landslides in the Auckland region utilising UAV/structure-from-motion photogrammetry. *Jpn. Geotech. Soc. Spec. Publ.* **2019**, *6*, 1–6. [CrossRef]
31. Avallone, A.; Briole, P.; Agatza-Balodimou, A.M.; Billiris, H.; Charade, O.; Mitsakaki, C.; Nercessian, A.; Papazissi, K.; Paradissis, D.; Veis, G. Analysis of eleven years of deformation measured by GPS in the Corinth Rift Laboratory area. *Comptes Rendus Geosci.* **2004**, *336*, 301–311. [CrossRef]
32. Fernández-Blanco, D.; de Gelder, G.; Lacassin, R.; Armijo, R. A new crustal fault formed the modern Corinth Rift. *Earth-Sci. Rev.* **2019**, *199*, 102919. [CrossRef]
33. Jolivet, L.; Labrousse, L.; Agard, P.; Lacombe, O.; Bailly, V.; Lecomte, E.; Mouthereau, F.; Mehl, C. Rifting and shallow-dipping detachments, clues from the Corinth Rift and the Aegean. *Tectonophysics* **2010**, *483*, 287–304. [CrossRef]
34. McKenzie, D. Active tectonics of the Alpine—Himalayan belt: The Aegean Sea and surrounding regions. *Geophys. J. Int.* **1978**, *55*, 217–254. [CrossRef]
35. Taylor, B.; Weiss, J.; Goodliffe, A.M.; Sachpazi, M.; Laigle, M.; Hirn, A. The structures, stratigraphy and evolution of the Gulf of Corinth rift, Greece. *Geophys. J. Int.* **2011**, *185*, 1189–1219. [CrossRef]
36. Micheletti, N.; Chandler, J.; Lane, S.N. Chapter 2—Structure from motion (SFM) photogrammetry. In *Geomorphological Techniques*; Section 2.2; British Society for Geomorphology: London, UK, 2015.
37. Smith, M.W.; Carrivick, J.L.; Quincey, D.J. Structure from motion photogrammetry in physical geography. *Prog. Phys. Geogr. Earth Environ.* **2016**, *40*, 247–275. [CrossRef]
38. Westoby, M.; Brasington, J.; Glasser, N.; Hambrey, M.; Reynolds, J. 'Structure-from-Motion' photogrammetry: A low-cost, effective tool for geoscience applications. *Geomorphology* **2012**, *179*, 300–314. [CrossRef]
39. Agisoft Metashape Professional Edition. Available online: https://www.agisoft.com/pdf/metashape-pro_1_7_en.pdf (accessed on 30 January 2022).
40. Nikolakopoulos, K.G.; Koukouvelas, I.K. Rockfalls systematic monitoring using UAVs: The case of Zachlorou village. In Proceedings of the Eighth International Conference on Remote Sensing and Geoinformation of the Environment (RSCy2020), Paphos, Cyprus, 16–18 March 2020. [CrossRef]
41. Brach, M.; Chan, J.C.-W.; Szymanski, P. Accuracy assessment of different photogrammetric software for processing data from low-cost UAV platforms in forest conditions. *iForest* **2019**, *12*, 435–441. [CrossRef]
42. Gindraux, S.; Boesch, R.; Farinotti, D. Accuracy Assessment of Digital Surface Models from Unmanned Aerial Vehicles' Imagery on Glaciers. *Remote Sens.* **2017**, *9*, 186. [CrossRef]
43. Nikolakopoulos, K.G.; Soura, K.; Koukouvelas, I.K.; Argyropoulos, N.G. UAV vs. classical aerial photogrammetry for archaeological studies. *J. Archaeol. Sci. Rep.* **2017**, *14*, 758–773. [CrossRef]
44. Agüera-Vega, F.; Carvajal-Ramírez, F.; Martínez-Carricondo, P. Assessment of photogrammetric mapping accuracy based on variation ground control points number using unmanned aerial vehicle. *Measurement* **2017**, *98*, 221–227. [CrossRef]
45. Akturk, E.; Altunel, A.O. Accuracy assessment of a low-cost UAV derived digital elevation model (DEM) in a highly broken and vegetated terrain. *Measurement* **2019**, *136*, 382–386. [CrossRef]
46. Ferrer-González, E.; Agüera-Vega, F.; Carvajal-Ramírez, F.; Martínez-Carricondo, P. UAV Photogrammetry Accuracy Assessment for Corridor Mapping Based on the Number and Distribution of Ground Control Points. *Remote Sens.* **2020**, *12*, 2447. [CrossRef]
47. Maurizio, B.; Fiani, M.; Lugli, A. Landslide monitoring using multitemporal terrestrial laser scanning for ground displacement analysis. *Geomat. Nat. Hazards Risk* **2015**, *6*, 398–418. [CrossRef]
48. Oppikofer, T.; Jaboyedoff, M.; Blikra, L.; Derron, M.-H.; Metzger, R. Characterization and monitoring of the Åknes rockslide using terrestrial laser scanning. *Nat. Hazards Earth Syst. Sci.* **2009**, *9*, 1003–1019. [CrossRef]
49. Rashidi, M.; Mohammadi, M.; Sadeghlou Kivi, S.; Abdolvand, M.M.; Truong-Hong, L.; Samali, B. A Decade of Modern Bridge Monitoring Using Terrestrial Laser Scanning: Review and Future Directions. *Remote Sens.* **2020**, *12*, 3796. [CrossRef]
50. Eker, R.; Aydın, A.; Hübl, J. Unmanned aerial vehicle (UAV)-based monitoring of a landslide: Gallenzerkogel landslide (Ybbs-Lower Austria) case study. *Env. Monit Assess* **2018**, *190*, 28. [CrossRef]

51. Fuad, N.A.; Yusoff, A.R.; Ismail, Z.; Majid, Z. Comparing the Performance of Point Cloud Registration Methods for Landslide Monitoring Using Mobile Laser Scanning Data. *ISPRS Int. Arch. Photogramm. Remote Sens. Spat. Inf. Sci.* **2018**, *4249*, 11–21. [CrossRef]
52. Martínez-Espejo Zaragoza, I.; Caroti, G.; Piemonte, A.; Riedel, B.; Tengen, D.; Niemeier, W. Structure from motion (SfM) processing of UAV images and combination with terrestrial laser scanning, applied for a 3D-documentation in a hazardous situation. Geomatics. *Nat. Hazards Risk* **2017**, *8*, 1492–1504. [CrossRef]
53. Wang GPhilips DJoyce, J.; Rivera, F. The Integration of TLS and Continuous GPS to Study Landslide Deformation: A Case Study in Puerto Rico. *J. Geod. Sci.* **2011**, *1*, 25–34. [CrossRef]
54. Zuliani, D.; Tunini, L.; Di Traglia, F.; Chersich, M.; Curone, D. Cost-Effective, Single-Frequency GPS Network as a Tool for Landslide Monitoring. *Sensors* **2022**, *22*, 3526. [CrossRef]
55. Šegina, E.; Peternel, T.; Urbančič, T.; Realini, E.; Zupan, M.; Jež, J.; Caldera, S.; Gatti, A.; Tagliaferro, G.; Consoli, A.; et al. Monitoring Surface Displacement of a Deep-Seated Landslide by a Low-Cost and near Real-Time GNSS System. *Remote Sens.* **2020**, *12*, 3375. [CrossRef]
56. Medjkane, M.; Maquaire, O.; Costa, S.; Roulland, T.; Letortu, P.; Fauchard, C.; Antoine, R.; Davidson, R. High-resolution monitoring of complex coastal morphology changes: Cross-efficiency of SfM and TLS-based survey (Vaches-Noires cliffs, Normandy, France). *Landslides* **2018**, *15*, 1097–1108. [CrossRef]
57. Cawood, A.J.; Bond, C.E.; Howell, J.A.; Butler, R.W.H.; Totake, Y. LiDAR, UAV or compassclinometer? Accuracy, coverage and the effects on structural models. *J. Struct. Geol.* **2017**, *98*, 67–82. [CrossRef]
58. Hugenholtz, C.H.; Whitehead, K.; Brown, O.W.; Barchyn, T.E.; Moorman, B.J.; LeClaire, A.; Riddell, K.; Hamilton, T. Geomorphological mapping with a small unmanned aircraft system (sUAS): Feature detection and accuracy assessment of a photogrammetrically-derived digital terrain model. *Geomorphology* **2013**, *194*, 16–24. [CrossRef]
59. Tonkin, T.N.; Midgley, N.G.; Graham, D.J.; Labadz, J.C. The potential of small unmanned aircraft systems and structure-from-motion for topographic surveys: A test of emerging integrated approaches at cwm Idwal, North Wales. *Geomorphology* **2014**, *226*, 35–43. [CrossRef]
60. Garcia, G.P.; Gomes, E.B.; Viana, C.D.; Grohmann, C.H. Comparing terrestrial laser scanner and UAV-based photogrammetry to generate a landslide dem. In *Anais do Xix Simpósio Brasileiro de Sensoriamento Remoto*; Santos. Anais eletrônicos. São José dos Campos, INPE, 2019. Proceedings of XIX Brazilian Symposium on Remote Sensing; ISBN 978-85-17-00097-3. Available online: https://proceedings.science/sbsr-2019/papers/comparing-terrestrial-laser-scanner-and-uav-based-photogrammetry-to-generate-a-landslide-dem?lang=en> (accessed on 31 July 2022).